ACS OMEGA

http://pubs.acs.org/journal/acsodf

Article

Investigation of Antibacterial Activity and Cell Viability of Ag/Mg and Ag/Zn Co-doped Hydroxyapatite Derived from Natural Limestone

Karya Sinulingga,* Makmur Sirait, Nurdin Siregar, and Maryati Evivani Doloksaribu

Cite This: *ACS Omega* 2021, 6, 34185−34191

Read Online

ACCESS | Metrics & More | Article Recommendations

ABSTRACT: Improving the antibacterial activity to avoid infections and keeping the biocompatibility at a safe level of HAp-based materials is highly important for biomedical applications. In this work, we investigate the antibacterial activity of 2.5Ag/2.5Mg co-doped HAp and 2.5Ag/2.5Zn co-doped HAp toward *Escherichia coli* bacteria. Moreover, their biocompatibility for osteoblastic cells (MC3T3-E1 cells) was also evaluated. The physical properties were characterized with necessary characterization tools such as X-ray diffraction, scanning electron microscopy, transmission electron microscopy, and Brunauer−Emmett−Teller. Both 2.5Ag/2.5Mg and 2.5Ag/2.5Zn co-doped HAp consist of hydroxyapatite (HAp) and beta calcium triphosphate (β-TCP) phases. The antibacterial test reveals that 2.5Ag/2.5Mg co-doped HAp or 2.5Ag/2.5Zn co-doped HAp has an outstanding antibacterial activity with a killing rate of 99 ± 1%. More importantly, the cell viability for osteoblast cells with 2.5Ag/2.5Mg and 2.5Ag/2.5Zn co-doped HAp promotes the proliferation much more effectively than 2.5Ag-doped HAp or 5Ag-doped HAp.

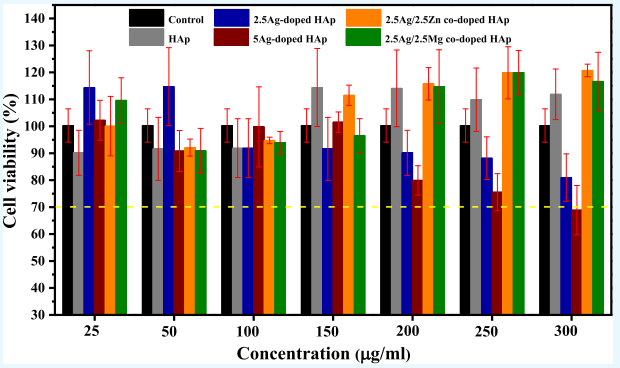

1. INTRODUCTION

Hydroxyapatite (HAp), one member of the calcium phosphate family, has received much attention due to its broad potential applications such as bone graft, dental implant, and so on.[1] Biocompatibility and biodegradability are two critical properties that a HAp-based material must possess for biomedical use. For a practical application, like surgery, the antibacterial capability is essential to prevent infection after treatment.[2,3] Unfortunately, pristine HAp has a low capability to deactivate bacteria.[4] Therefore, improving the antibacterial activity to avoid using antibiotics and keeping the biocompatibility safe for human tissue is an essential task for researchers and scientists.

In the last few decades, numerous reports investigated how to improve the antibacterial properties of HAp by a doping technique with different metal ions such as silver, copper, zinc, magnesium, and so forth.[5−8] Among them, silver (Ag) is the most widely used as a dopant to enhance not only the antibacterial activity but also antifungal capability.[9,10] Ag ions have a vital role in interacting with the cell membrane of bacteria via electrostatic attraction and then leading to the destruction of the cell membrane.[11] At a low concentration, the Ag ions would replace some of the Ca ions in the HAp matrix without changing the crystal structure.[12] Unfortunately, a Ag-doped HAp material could be toxic to the cells at a high Ag concentration, which is called cytotoxicity.[13] Moreover, Costescu et al. have also reported that too high Ag-ion concentrations could decrease the performance.[14] Based on this consideration, it is important to control the Ag concentration in the HAp matrix at a safe level but at the same time Ag-HAp also should have great antibacterial capability and cell viability. Incorporating a second metal into the Ag-HAp system, known as the co-doping technique, is one of the best strategies to achieve that aforementioned goal. Because the human bone consists of several metal ions such as Zn and Mg, they have potential to improve the osteoplastic cell.[15,16]

In the previous work, we have successfully synthesized HAp by utilizing natural limestone as the calcium source.[17] Limestone, one of the most abundant minerals on earth, possesses a high calcium content (ca. 40%) with the benefit of low cost as compared to the chemical synthesis. The antibacterial activity of that HAp was also highly enhanced

Received: October 22, 2021
Accepted: November 16, 2021
Published: November 30, 2021

by doping with 5% Ag metal ions. Although its antibacterial activity was great, Ag is well known as a high-cost material and has toxicity issues for the human body. Therefore, it is important to reduce the Ag content in order to lower the cost without degrading the antibacterial activity. In this work, we further investigate the antibacterial activity of HAp by incorporating two metal ions simultaneously (2.5Ag/2.5Zn and 2.5Ag/2.5Mg co-doped HAp). Moreover, the biocompatibility of co-doped HAp materials as one of the critical properties for bone graft is also tested and compared for osteoblastic cells (MC3T3-E1 cell). We find that both 2.5Ag/2.5Zn and 2.5Ag/2.5Mg co-doped HAp have a great antibacterial activity of 99 ± 1%. More importantly, the incorporation of Zn or Mg significantly improves the cell viability especially at a high concentration of 300 μg/mL.

2. RESULTS AND DISCUSSION

2.1. X-ray Diffraction Analysis. An X-ray diffractometer with an accelerating voltage of 30 kV was employed to identify the crystal structure and phase of co-doped HAp. First, it is important to discuss the X-ray diffraction pattern of undoped HAp. As shown in Figure 1, the X-ray diffraction of undoped

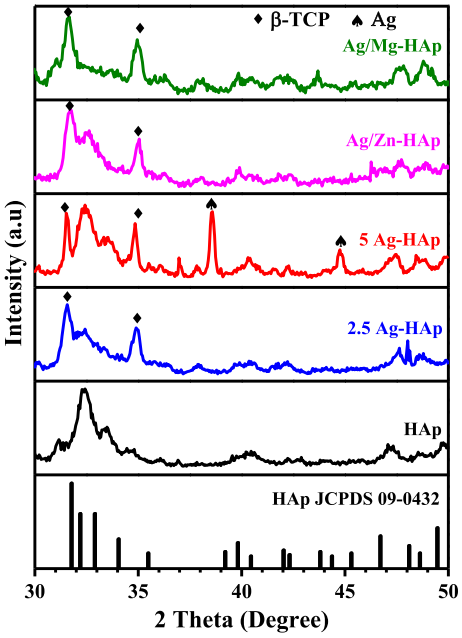

Figure 1. X-ray diffraction patterns of pristine HAp, 2.5Ag-doped HAp, 5Ag-HAp, 2.5Ag/2.5Zn co-doped HAp, and 2.5Ag/2.5Mg co-doped HAp.

HAp totally fit to the hydroxyapatite according to JCPDS. 09-3420. There is no other peak observable which indicates that undoped HAp has high purity. However, after doping with 5% Ag (5Ag-doped HAp), there are several new peaks that appear as compared to that undoped HAp. Those peaks located at 38.4 and 44.5° could be attributed to the presence of Ag metal, while the other peaks at 31.3 and 33.6° could be assigned to the presence of the beta calcium triphosphate (β-TCP) phase. This phenomenon occurred due to the reduction of Ag ions under a high-temperature process, as we have comprehensively explained in our previous report.[17] Interestingly, when the concentration of Ag is reduced to 2.5%, the X-ray diffraction remains identical to that of 5Ag-doped HAp, but there are no peaks at 38.4 and 44.5° for 2θ. Because the Ag concentration is now significantly lower than that 5Ag-doped HAp, the Ag did not precipitate as Ag metal; instead, all the Ag ions occupied the Ca sides in the HAp and or the β-TCP matrix. Both 2.5Ag/2.5Zn and 2.5Ag/2.5Mg co-doped HAp have X-ray diffraction patterns that are quite similar to the pattern of that 2.5Ag-HAp, which consists of HAp and β-TCP phases without any other impurity. The presence of those phases in a single material is also known as biphasic calcium phosphate (BCP).[18] The size of the crystallite was calculated based on the Scherer equation which depended on the full-width half maximum (FWHM) and diffraction angle (θ).[19] Table 1 lists the

Table 1. FWHM and Crystallite Sizes of 2.5Ag-Doped HAp, 2.5Ag/2.5Mg Co-doped HAp and 2.5Ag/2.5Zn Co-doped HAp

samples	FWHM	crystallite size (nm)
2.5Ag-doped HAp	0.230	36.40
2.5Ag/2.5Zn co-doped HAp	0.507	16.18
2.5Ag/2.5Mg co-doped Hap	0.847	9.66

crystallite size of 2.5Ag-HAp, 2.5Ag/2.5Zn, and 2.5Ag/2.5Mg co-doped HAp. The crystallite size of 2.5Ag-doped HAp was 36.4 nm. However after co-doping, the crystallite size significantly decreased to 16.18 and 9.66 nm for 2.5Ag/2.5Zn and 2.5Ag/2.5Mg co-doped HAp, respectively. The decrease of the crystallite size indicates more defects as the second metal ions of Zn and Mg were successfully doped into the HAp matrix.[20]

2.2. Electron Microscopy and Element Composition Analyses. The surface morphologies of 2.5Ag-HAp, 2.5Ag/2.5Mg co-doped HAp, and 2.5Ag/2.5Zn co-doped HAp were first recorded using a field-emission scanning electron microscope. Figure 2a shows that the morphology of 2.5Ag-doped HAp consists of agglomerated particles. The morphology of 2.5Ag/2.5Mg co-doped HAp and 2.5Ag/2.5Zn co-doped HAp in Figure 2b,c is not much different as compared to that of 2.5Ag-doped HAp. To further observe more clearly the microstructure, transmission electron microscopy (TEM) analysis was further conducted with an accelerating voltage of 200 kV. As exhibited in Figure 2d−f, it is clearly observed that all samples have a similar irregular shape and contain a lot of tiny particles.

The element composition was investigated by energy-dispersive X-ray spectroscopy (EDS). The EDS spectra of 2.5Ag-doped HAp, 2.5Ag/2.5Mg co-doped Hap, and 2.5Ag/2.5Zn co-doped HAp in Figure 3a−c show several peaks, including phosphor (P), calcium (Ca), oxygen (O), silver (Ag), zinc (Zn), and magnesium (Mg), which reveals the presence of metal-ion dopants. It is reasonable that the peak intensity of Ag, Zn, and Mg is much lower as compared to the peak intensity of Ca due to a low concentration. Furthermore, the quantitative EDS results are tabulated in Table 2. The molar percentage of Ag as a metal dopant in 2.5Ag-doped HAp was 0.97%, while the molar percentages of Ca, P, and O were 21.86, 13.06, and 64.12%, respectively. As also can be seen in Table 2, the atomic concentration of Mg and Ag as the co-dopants in 2.5Ag/2.5Mg co-doped HAp is 0.82 and 0.59%, respectively. The composition of 2.5Ag/2.5Zn co-doped HAp is similar to that of 2.5Ag/2.5Mg co-doped with concentrations of 0.80 and 0.69% for Zn and Ag, respectively. It is found that the concentration of Ag is slightly lower in both 2.5Ag/2.5Mg

https://doi.org/10.1021/acsomega.1c05921
ACS Omega 2021, 6, 34185−34191

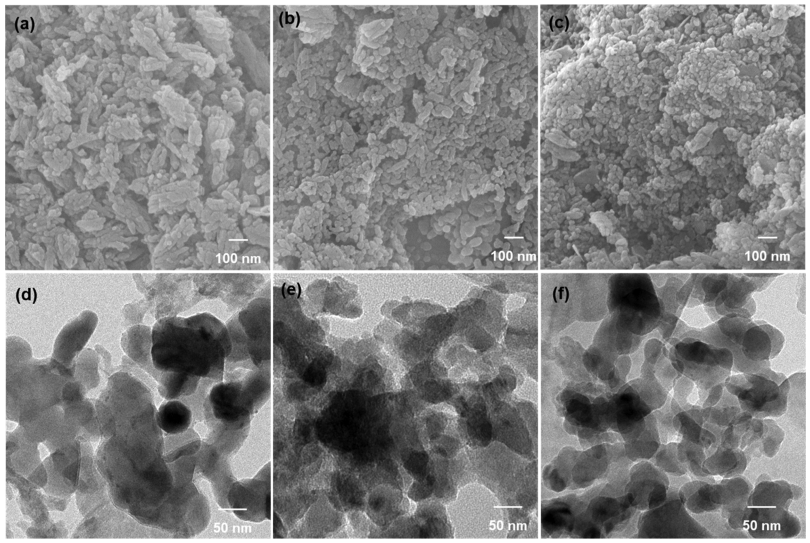

Figure 2. Scanning electron microscopy (SEM) and TEM images of (a, d) 2.5Ag-HAp, (b, e) 2.5Ag/2.5Mg co-, and (c, f) 2.5Ag/2.5Zn co-doped HAp.

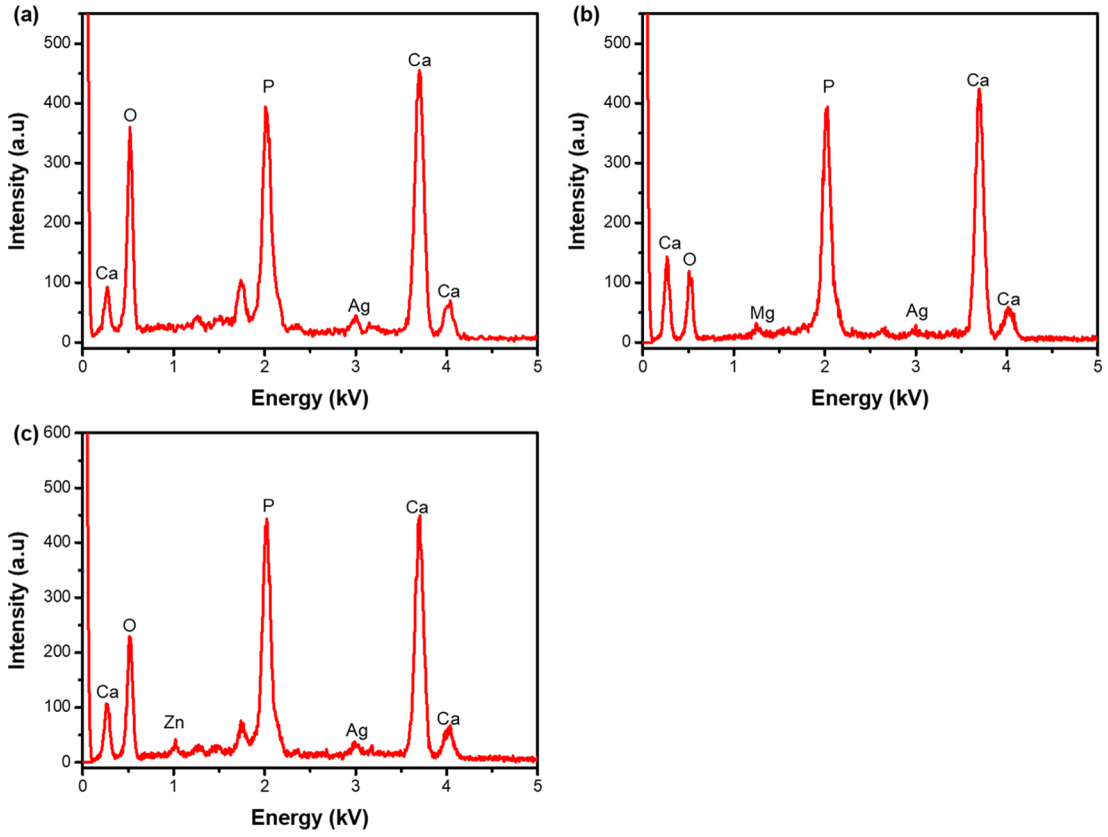

Figure 3. EDS spectra of (a) 2.5Ag-HAp, (b) 2.5Ag/2.5Mg co-doped HAp, and (c) 2.5Ag/2.5Zn co-doped HAp.

Table 2. Atomic Percentage Results for 2.5Ag-Doped HAp, 2.5Ag/2.5Zn Co-doped HAp, and 2.5Ag/2.5Mg Co-doped HAp

samples	Zn	Mg	Ag	Ca	P	O
2.5Ag-HAp			0.97	21.86	13.06	64.11
2.5Ag/2.5Mg-HAp		0.82	0.59	21.91	15.05	61.63
2.5Ag/2.5Zn-HAp	0.80		0.69	21.79	14.79	61.78

and 2.5Ag/2.5Zn co-doped HAp as compared to that 2.5Ag-doped HAp.

2.3. BET Analysis. The surface area is one of the important properties of nano-HAp-based materials because it could affect the antibacterial properties.[9] As shown in Table 3, the surface area of undoped HAp is only about 21.9 m^2/g. After doping with 2.5% Ag, the surface area greatly improved by 1.7-fold as compared to undoped HAp. However, the incorporation of Zn or Mg as the second dopant did not significantly change the surface area. The surface areas of 2.5Ag/2.5Mg and 2.5Ag/

https://doi.org/10.1021/acsomega.1c05921
ACS Omega 2021, 6, 34185−34191

Table 3. Surface Area and Pore Size of HAp, 2.5Ag-Doped HAp, 2.5Ag/2.5Zn Co-doped HAp, and 2.5Ag/2.5Mg Co-doped HAp

samples	specific surface area (m^2/g)	average pore size (nm)
HAp	21.9	1.6
2.5Ag-doped HAp	37.6	1.7
2.5Ag/2.5Mg co-doped HAp	39.4	1.6
2.5Ag/2.5Zn co-doped HAp	38.2	1.7

2.5Zn co-doped HAp were 39.3 and 38.2 m^2/g, respectively. The pore size of undoped 2.5Ag-HAp and 2.5Ag/2.5Zn or 2.5Ag/2.5Mg co-doped HAp was close to each other with a range of 1.6−1.7 nm. To further determine the mesoporous type, the nitrogen absorption−desorption experiment was performed at a constant temperature. As presented in Figure 4a−c, the curves are quite similar and indicate that our 2.5Ag/2.5Zn and 2.5Ag/2.5Mg co-doped HAp belong to type IV mesopore materials.[21] Furthermore, the pore size distribution in Figure 4d−f clearly indicates that 2.5Ag-HAp and 2.5Ag/2.5Zn co-doped HAp and 2.5Ag/2.5Mg co-doped HAp have pore sizes below 10 nm, which further confirms the mesopore properties of our HAp-based materials.

2.4. Antibacterial Activity. The antibacterial capability of pristine HAp, 2.5Ag-HAp, 5Ag-HAp, 2.5Ag/2.5Zn co-doped HAp, and 2.5Ag/2.5Mg co-doped HAp were evaluated toward *Escherichia coli* bacteria. Figure 5 exhibits the photograph of the bacterial test after 24 h under the dark conditions. The antibacterial rate is then calculated and plotted in Figure 6. The pristine HAp showed a low antibacterial activity with a percentage of 12 ± 9%. However, the Ag doped-HAp sample with a low Ag content of 2.5% had much higher activity with a rate of 61 ± 9%. As expected, with a higher Ag content, the 5Ag-doped HAp sample had a 99 ± 1% antibacterial activity. Interestingly, both 2.5Ag/2.5Zn co-doped HAp and 2.5Ag/2.5Mg co-doped HAp also exhibited 99 ± 1% antibacterial activity. This result indicates that both 2.5Ag/2.5Zn co-doped HAp and 2.5Ag/2.5Mg co-doped HAp have great potential for deactivating *E. coli* bacteria, which was attributed to more interaction between metal ions and the bacterial wall membranes via an electrostatic force or reactive oxygen species (ROS) to damage the cell membrane.[9,22]

2.5. Cell Viability. Cytotoxicity and biocompatibility are extremely important properties for practical biomedical applications.[23] The cytotoxicities of our HAp, 2.5Ag-HAp, 5Ag-HAp, 2.5Ag/2.5Zn co-doped HAp, and 2.5Ag/2.5Mg co-doped HAp were then evaluated by using the MTT assay on MC3T3-E1 cells. Figure 7 shows the results for different extraction concentrations of 25, 50, 100, 150, 200, 250, and 300 μg/mL after 72 h of incubation. It is well known that standard cell viability according to ISO 10993-5 is ≥ 70%.[24] The cell viability data in Figure 6 clearly exhibit that almost all samples have a cell viability over 70% even for the highest extract concentration of 300 μg/mL, except for the 5Ag-doped HAp sample. At a concentration less than 200 μg/mL, 5Ag-doped HAp had cell viability below 70%. However, when the extract concentration increases to 250 and 300 μg/mL, the cell viability gradually decreased to 75 ± 7 and 68 ± 9%, respectively. These data reveal that 5Ag-doped has high potential of cytotoxicity effect on the MC3T3-E1 cells. The calculated cell viability of 2.5Ag/2.5Zn co-doped HAp and 2.5Ag/2.5Mg co-doped HAp for a high extract concentration of 300 μg/mL were 120 ± 2 and 116 ± 10%, respectively, which were much higher than that of 5Ag-doped HAp (68 ± 9%). It should be emphasized that our strategy of replacing some Ag ions with Zn or Mg metal ions as the second metal

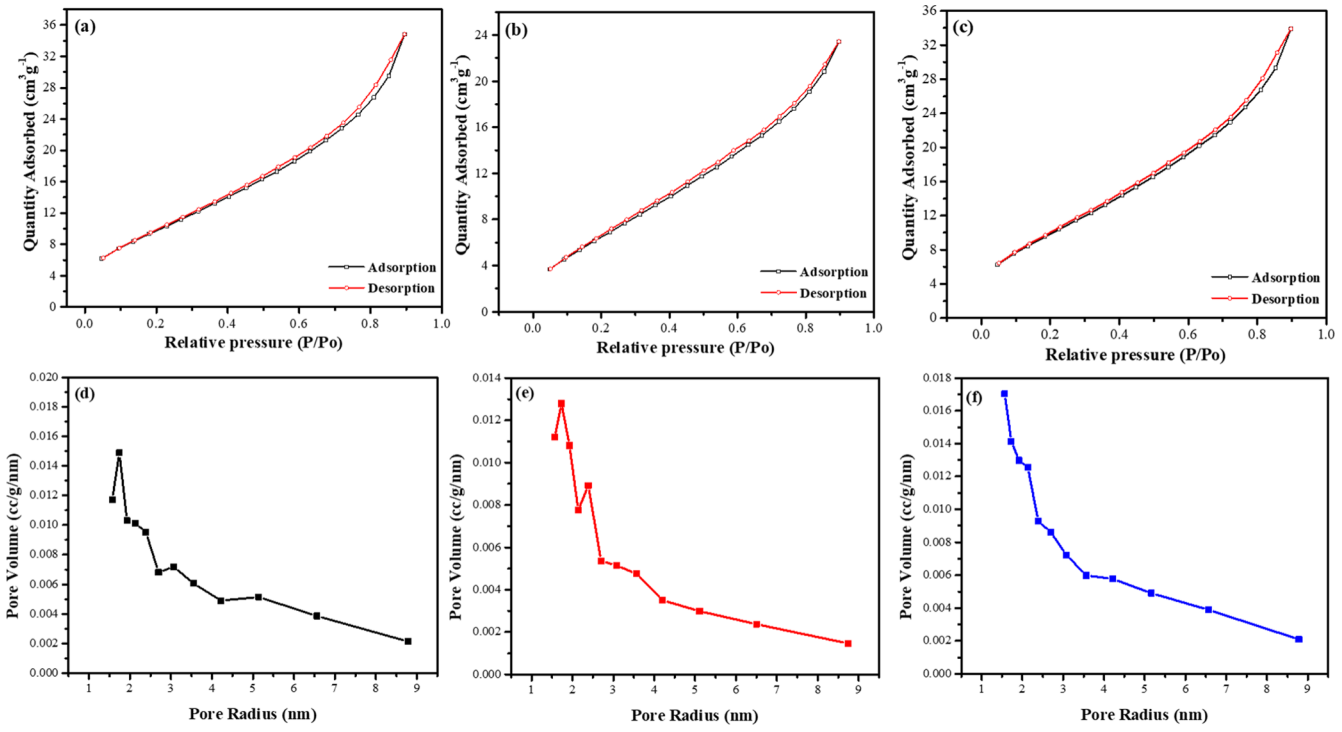

Figure 4. Nitrogen absorption−desorption curve and pore size distribution (a, d) 2.5Ag-doped HAp, (b, e) 2.5Ag/2.5Zn co-doped HAp, and (c, f) 2.5Ag/2.5Mg co-doped HAp.

https://doi.org/10.1021/acsomega.1c05921
ACS Omega 2021, 6, 34185−34191

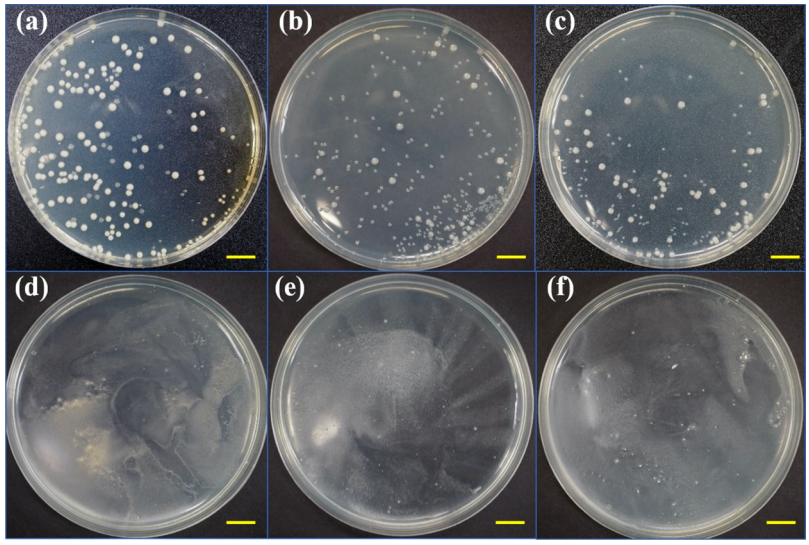

Figure 5. Photograph images of the antibacterial tests of (a) control, (b) pristine HAp, (c) 2.5Ag-HAp, (d) 5Ag-HAp, (e) 2.5Ag/2.5Zn co-doped HAp, and (f) 2.5Ag/2.5Mg co-doped HAp against *E. coli*. Note: the scale bar is 1 cm.

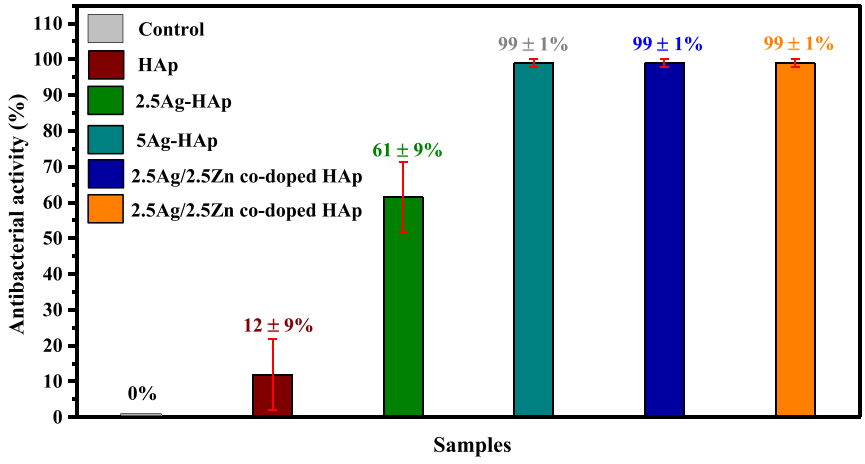

Figure 6. Histogram of antibacterial activities toward *E. coli* in the presences of pristine HAp, 2.5Ag-doped HAp, 5Ag-doped HAp, 2.5Ag/2.5Zn co-doped HAp, and 2.5Ag/2.5Mg co-doped HAp.

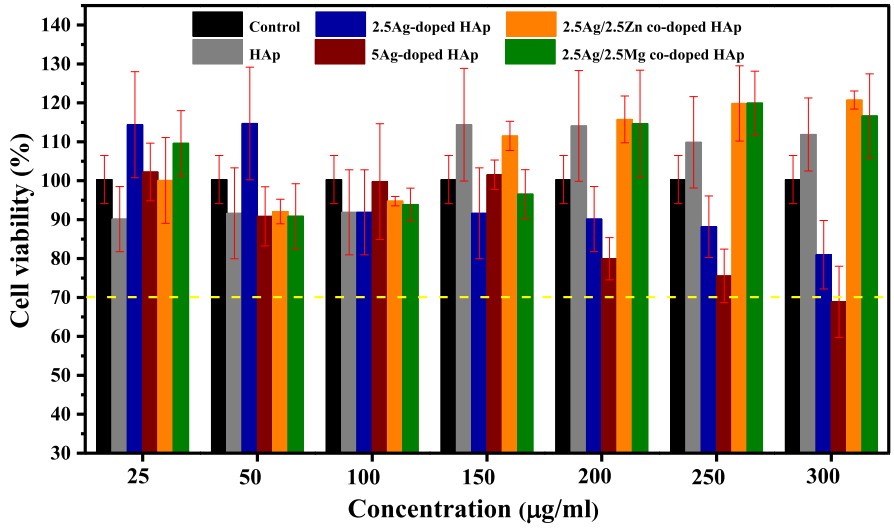

Figure 7. Cell viability analysis for pristine HAp, 2.5Ag-doped HAp, 5Ag-doped HAp, 2.5Ag/2.5Zn co-doped HAp, and 2.5Ag/2.5Mg co-doped HAp.

https://doi.org/10.1021/acsomega.1c05921
ACS Omega 2021, 6, 34185−34191

dopant has proved to promote the proliferation much more effectively than that with 2.5Ag-doped HAp and 5Ag-doped HAp. The previous studies suggested that the presence of Mg ions and Zn ions in the HAp structure had an important role in enhancing the osteoconductivity and resorption properties.[15,25] Based on these results, our 2.5Ag/2.5Zn co-doped HAp and 2.5Ag/2.5Mg co-doped HAp are suitable for biomedical applications not only due to their great biocompatibility but also excellent antibacterial activity. Furthermore, our co-doping strategy in this work has another advantage of reducing the cost as the price of Mg or Zn metal is much cheaper than the price of Ag.

3. CONCLUSIONS

2.5Ag/2.5Mg co-doped HAp and 2.5Ag/2.5Zn co-doped HAp have been successfully prepared using a sol-gel method followed by thermal annealing at 700 °C. The XRD analysis revealed that both 2.5Ag/2.5Mg and 2.5Ag/2.5Zn co-doped HAp possessed HAp and β-TCP phases. The BET analysis confirmed that our co-doped HAp was a type IV mesoporous material with a surface area of 40 m^2/g and an average pore size of 1.6 nm. The antibacterial activity test showed that 2.5Ag/2.5Mg co-doped HAp and 2.5Ag/2.5Zn co-doped HAp had an outstanding bacterium killing rate of 99 ± 1% toward *E. coli*. More importantly, the cell viability test on osteoblast cells (MC3T3-E1) revealed that co-doping HAp had no cytotoxic effect and it was able to improve cell growth. This report shows that using the co-doping strategy with proper dopants not only can improve the antibacterial activity but also enhance the growth of the osteoblastic cells.

4. EXPERIMENTAL SECTION

4.1. Synthesis of 2.5Ag/2.5Zn Co-Doped HAp and 2.5Ag/2.5Mg Co-Doped HAp. Pristine HAp and Ag-doped HAp were prepared by similar procedures to our previous report.[17] 2.5Ag/2.5Zn co-doped HAp and 2.5Ag/2.5Mg co-doped HAp were also synthesized by a similar method. First, 5.6 g of CaO obtained by heating limestone ($CaCO_3$) at 900 °C for 5 h was added into 500 mL of deionized (DI) water under constant stirring. After stirring for several hours, $Ca(OH)_2$ was successfully produced. Then, 2.5% $AgNO_3$ and 2.5% $Zn(NO_3)_2$ (denoted as 2.5Ag/2.5Zn co-doped HAp) or 2.5% $Mg(NO_3)_2$ (denoted as 2.5Ag/2.5Mg co-doped HAp) was added into that previous solution. After that, 3.1 mL of phosphoric acid was slowly added under continuous stirring for 4 h. The obtained gel was then collected by centrifugation. After the drying process, the sample was annealed in a muffle furnace at 700 °C for 2 h.

4.2. Characterizations. X-ray diffractometry (D2 Phaser) was used to investigate the crystal property of 2.5Ag/2.5Zn and 2.5Ag/2.5Mg co-doped HAp. A field-emission scanning electron microscope (JSM 6500F) was used to observe the morphology. TEM (JEOL, 2100) was also further employed to investigate the microstructure. The element composition was investigated using EDS and analyzed using an integrated calibration tool (INCA software, Oxford instrument). Nitrogen absorption and desorption isotherm experiments were conducted using Brunauer−Emmet−Teller (BET) analysis (Novatouch LX2, Quantachrome Instrument) to measure the specific surface area, average pore size, and pore size distribution.

4.3. Antibacterial Activity. The antibacterial properties of the as-synthesized HAp-based materials were evaluated against gram-negative bacteria *E. coli* bacteria. The plate count technique (ASTM International E3031-15) was used to evaluate bacterial activity. Bacteria were initially inoculated overnight at 37 °C in Luria-Bertani (LB) medium. The bacteria were then diluted in a phosphate-buffered saline solution. After that, 1 mg of the as-prepared HAp-based samples was added into 0.5 mL of the diluted bacteria solution (10^3 colony-forming unit, CFU) and then was spread on a petri dish with agar medium. Finally, it was incubated at 37 °C for 24 h. The bacteria were counted using a colony counter machine (Rocker galaxy 330, Kaohsiung, Taiwan), and the results were compared to the control experiment without any sample or pure bacteria. On the basis of the colony numbers, the antibacterial activity was determined using the equation below:

$$R = [(A - B)/A] \times 100\%$$

where R is the antibacterial killing rate (in percent), A is the average number of bacteria (in CFU) in the control experiment, and B is the average number of bacteria in the testing sample. The measurements were repeated three times to obtain the accurate result.

4.4. Cell Viability (MTT Test). The isolated osteoblastic cells (MC3T3-E1 cell line ATCC CRL-2594, Virginia, USA) were cultured in 75 cm^2 cell culture flasks containing minimum essential medium (MEM α, Gibco, Massachusetts, USA) supplemented with 10% fetal bovine serum (FBS, Gibco, Massachusetts, USA) and 1% antibiotic-antimycotic (Corning, New York, USA) maintained at 37 °C in an incubator with a 5% CO_2 humidified atmosphere. To assess the cell viability effect, a 500 μL suspension of MC3T3-E1 cells was seeded into 24-well plates at a density of 2×10^4 cells/well and incubated for 1 day to allow the adherence of the cells. Afterward, the toxicity of MC3T3-E1 cells was investigated on HAp, 2.5Ag-, 5Ag-, AgZn co-doped, and Ag/Mg co-doped HAp with various concentrations (25, 50, 100, 150, and 200 μg/mL) of the extract solution added to each well. Cells without sample extract dilution were used as a control. Each sample concentration was prepared in triplicate. After 3 days of incubation, the medium was aspirated from all wells, and 200 μL of thiazolyl blue tetrazolium bromide MTT (L119139, Alfa aesar, Massachusetts, USA) solutions was added to each well and incubated for another 4 h to form formazan. At the end of the incubation period, the MTT solution was removed, and 300 μL of dimethyl sulfoxide (DMSO, ECHO, Taiwan) was added to each well. The solution was transferred to a 96-well plate, and the absorbance was measured at 570 nm using a microplate reader (Multiskan Go, Thermo Scientific, USA). The cell viability percentage of each concentration was calculated by assuming the cell viability of the control as 100%.).

AUTHOR INFORMATION

Corresponding Author

Karya Sinulingga − *Department of Physics, Faculty of Mathematics and Natural Sciences, Universitas Negeri Medan, Medan 20221, Indonesia*;
Email: karyasinulinggakarya@unimed.ac.id

https://doi.org/10.1021/acsomega.1c05921
ACS Omega 2021, 6, 34185−34191

Authors

Makmur Sirait − *Department of Physics, Faculty of Mathematics and Natural Sciences, Universitas Negeri Medan, Medan 20221, Indonesia*

Nurdin Siregar − *Department of Physics, Faculty of Mathematics and Natural Sciences, Universitas Negeri Medan, Medan 20221, Indonesia*

Maryati Evivani Doloksaribu − *Department of Physics, Faculty of Mathematics and Natural Sciences, Universitas Negeri Medan, Medan 20221, Indonesia*

Complete contact information is available at: https://pubs.acs.org/10.1021/acsomega.1c05921

Notes

The authors declare no competing financial interest.

■ ACKNOWLEDGMENTS

This work was supported by the directorate general of higher education, ministry of education of the republic of Indonesia under grant number 123/UN33.8/KEP/PPKM/2021. The author's gratitude goes to the rector of the State University of Medan and chairman of the research and development of the State University of Medan.

■ REFERENCES

(1) Nga, N. K.; Thuy Chau, N. T.; Viet, P. H. Facile synthesis of hydroxyapatite nanoparticles mimicking biological apatite from eggshells for bone-tissue engineering. *Colloids Surf., B* **2018**, *172*, 769−778.

(2) Guo, X.; Cao, B.; Wang, C.; Lu, S.; Hu, X. In vivo photothermal inhibition of methicillin-resistantStaphylococcus aureusinfection byin situtemplated formulation of pathogen-targeting phototheranostics. *Nanoscale* **2020**, *12*, 7651−7659.

(3) Cao, B.; Lyu, X.; Wang, C.; Lu, S.; Xing, D.; Hu, X. Rational collaborative ablation of bacterial biofilms ignited by physical cavitation and concurrent deep antibiotic release. *Biomaterials* **2020**, *262*, 120341.

(4) Iqbal, N.; Kadir, M. R. A.; Mahmood, N. H.; Salim, N.; Froemming, G. R. A.; Balaji, H. R.; Kamarul, T. Characterization, antibacterial and in vitro compatibility of zinc-silver doped hydroxyapatite nanoparticles prepared through microwave synthesis. *Ceram. Int.* **2014**, *40*, 4507−4513.

(5) Predoi, D.; Iconaru, S. L.; Predoi, M. V. Fabrication of Silver- and Zinc-Doped Hydroxyapatite Coatings for Enhancing Antimicrobial Effect. *Coatings* **2020**, *10*, 905.

(6) Predoi, D.; Iconaru, S. L.; Predoi, M. V.; Stan, G. E.; Buton, N. Synthesis, Characterization, and Antimicrobial Activity of Magnesium-Doped Hydroxyapatite Suspensions. *Nanomaterials* **2019**, *9*, 1295.

(7) Ofudje, E. A.; Adeogun, A. I.; Idowu, M. A.; Kareem, S. O. Synthesis and characterization of Zn-Doped hydroxyapatite: scaffold application, antibacterial and bioactivity studies. *Heliyon* **2019**, *5*, No. e01716.

(8) Jadalannagari, S.; Deshmukh, K.; Ramanan, S. R.; Kowshik, M. Antimicrobial activity of hemocompatible silver doped hydroxyapatite nanoparticles synthesized by modified sol-gel technique. *Appl. Nanosci.* **2014**, *4*, 133−141.

(9) Hou, Y.-X.; Abdullah, H.; Kuo, D.-H.; Leu, S.-J.; Gultom, N. S.; Su, C.-H. A comparison study of SiO 2 /nano metal oxide composite sphere for antibacterial application. *Composites, Part B* **2018**, *133*, 166−176.

(10) Qasim, M.; Udomluck, N.; Chang, J.; Park, H.; Kim, K. Antimicrobial activity of silver nanoparticles encapsulated in poly-N-isopropylacrylamide-based polymeric nanoparticles. *Int. J. Nanomed.* **2018**, *13*, 235−249.

(11) Kędziora, A.; Speruda, M.; Krzyżewska, E.; Rybka, J.; Łukowiak, A.; Bugla-Płoskońska, G. Similarities and Differences between Silver Ions and Silver in Nanoforms as Antibacterial Agents. *Int. J. Mol. Sci.* **2018**, *19*, 444.

(12) Orlovskii, V. P.; Komlev, V. S.; Barinov, S. M. Hydroxyapatite and Hydroxyapatite-Based Ceramics. *Inorg. Mater.* **2002**, *38*, 973−984.

(13) Chen, K.; Ustriyana, P.; Moore, F.; Sahai, N. Biological Response of and Blood Plasma Protein Adsorption on Silver-Doped Hydroxyapatite. *ACS Biomater. Sci. Eng.* **2019**, *5*, 561−571.

(14) Costescu, A.; Ciobanu, C. S.; Iconaru, S. L.; Ghita, R. V.; Chifiriuc, C. M.; Marutescu, L. G.; Predoi, D. Fabrication, characterization, and antimicrobial activity, evaluation of low silver concentrations in silver-doped hydroxyapatite nanoparticles. *J. Nanomater.* **2013**, *2013*, 1−9.

(15) Bhattacharjee, P.; Begam, H.; Chanda, A.; Nandi, S. K. Animal trial on zinc doped hydroxyapatite: A case study. *Journal of Asian Ceramic Societies* **2014**, *2*, 44−51.

(16) Andrés, N. C.; Sieben, J. M.; Baldini, M.; Rodríguez, C. H.; Famiglietti, Á.; Messina, P. V. Electroactive Mg2+-Hydroxyapatite Nanostructured Networks against Drug-Resistant Bone Infection Strains. *ACS Appl. Mater. Interfaces* **2018**, *10*, 19534−19544.

(17) Sinulingga, K.; Sirait, M.; Siregar, N.; Abdullah, H. Synthesis and characterizations of natural limestone-derived nano-hydroxyapatite (HAp): a comparison study of different metals doped HAps on antibacterial activity. *RSC Adv.* **2021**, *11*, 15896−15904.

(18) Kim, D.-H.; Hwang, K.-H.; Lee, J. D.; Park, H.-C.; Yoon, S.-Y. Long and short range order structural analysis of In-situ formed biphasic calcium phosphates. *Biomater. Res.* **2015**, *19*, 14.

(19) Gultom, N. S.; Abdullah, H.; Kuo, D.-H. Phase transformation of bimetal zinc nickel oxide to oxysulfide photocatalyst with its exceptional performance to evolve hydrogen. *Appl. Catal., B* **2020**, *272*, 118985.

(20) Zeleke, M. A.; Kuo, D.-H.; Ahmed, K. E.; Gultom, N. S. Facile synthesis of bimetallic (In,Ga)2(O,S)3 oxy-sulfide nanoflower and its enhanced photocatalytic activity for reduction of Cr(VI). *J. Colloid Interface Sci.* **2018**, *530*, 567−578.

(21) Gultom, N. S.; Abdullah, H.; Xie, J.-C.; Kuo, D.-H. Transforming Zn(O,S) from UV to visible-light-driven catalyst with improved hydrogen production rate: Effect of indium and heterojunction. *J. Alloys Compd.* **2021**, *869*, 159316.

(22) Feng, Q. L.; Wu, J.; Chen, G. Q.; Cui, F. Z.; Kim, T. N.; Kim, J. O. A mechanistic study of the antibacterial effect of silver ions onEscherichia coli andStaphylococcus aureus. *J. Biomed. Mater. Res.* **2000**, *52*, 662−668.

(23) Büyüksağiş, A.; Çiftçi, N. HAP Coatings for Biomedical Applications: Biocompatibility and Surface Protection Against Corrosion of Ti, Ti6Al4V and AISI 316L SS. *Prot. Met. Phys. Chem. Surf.* **2020**, *56*, 834−843.

(24) Wallin, R. F. *A Practical Guide to ISO 10993-5: Cytotoxicity*, 1998; *20*, pp 96−98.

(25) Landi, E.; Logroscino, G.; Proietti, L.; Tampieri, A.; Sandri, M.; Sprio, S. Biomimetic Mg-substituted hydroxyapatite: from synthesis to in vivo behaviour. *J. Mater. Sci.: Mater. Med.* **2008**, *19*, 239−247.